Journal of the European Ceramic Society **10** (1992) 175–193

Interfacial Boundaries in Si_3N_4-Based Ceramic Composites: Constraints from Matrix Effects and Stability of Microstructure

W. Braue

German Aerospace Research Establishment (DLR), Materials Research Institute, Linder Höhe, D-5000 Cologne 90, Germany

(Received 17 February 1992; accepted 24 April 1992)

Abstract

The stability of the microstructure of Si_3N_4-based composites with discontinuous SiC reinforcement components (whiskers, platelets) is addressed, focusing on the role of interfacial boundaries. This approach basically explores four issues:

(1) The evaluation of structural configuration and interfacial chemistry of internal interfaces by means of HREM imaging and parallel detection electron energy loss spectroscopy (PEELS), considering the effects of different oxygen sources in the SiC/Si_3N_4 system.

(2) The influence of whisker-related impurities, such as excess carbon and oxygen, on the liquid-phase formation process and microstructural development of the Si_3N_4 baseline material.

(3) The variety of local microstructures along interfacial boundaries in Si_3N_4-based composites employing SiC-whiskers, -platelets and -fibers due to thermodynamic constraints which emphasize the dynamic nature of internal interfaces in ceramic matrix composites.

(4) The fundamental problem of correlating microscopic characteristics from grain and phase boundaries with the fracture resistance behavior of composite materials, considering that macroscopic, matrix-related parameters contribute to the mechanical response.

Die Arbeit diskutiert die Gefügestabilität von Verbundwerkstoffen auf Si_3N_4-Basis mit diskontinuierlichen SiC-Verstärkungskomponenten (Whisker, Platelets) unter besonderer Berücksichtigung der inneren Grenzflächen. Dabei stehen vier Themenkreise im Vordergrund:

(1) Die Bestimmung von Struktur und chemischer Zusammensetzung innerer Grenzflächen mit Hilfe der hochauflösenden Transmissionselektronenmikroskopie (HREM) sowie der Elektronenenergieverlustspektroskopie in Paralleldetektion (PEELS), wobei in SiC/Si_3N_4 Materialien mehrere Sauerstoffquellen berücksichtigt werden müssen.

(2) Der Einfluß von whiskerspezifischen Verunreinigungen, wie z.B. überschüssigem Kohlenstoff und Sauerstoff, auf den Flüssigphasensinterprozeß und die Gefügeentwicklung des monolithischen Si_3N_4-Materials.

(3) Die Vielfalt lokaler Gefügezustände entlang innerer Grenzflächen in Si_3N_4-Verbundwerkstoffen mit SiC-Whiskern, -Platelets und -Fasern aufgrund thermodynamischer Kriterien, die letztlich den dynamischen Charakter solcher Grenzflächen unterstreichen.

(4) Die grundlegende Problematik, mikroskopische Eigenschaften von Korn- und Phasengrenzen mit dem Bruchwiderstand von Verbundwerkstoffen zu korrelieren, wenn dieses mechanische Verhalten zudem noch von makroskopischen, matrixbezogenen Parametern bestimmt wird.

La stabilité microstructurale de composites à base de Si_3N_4 renforcés par une distribution discontinue de composés en SiC (whiskers, plaquettes) est examinée en se focalisant sur le rôle des liaisons interfaciales.

Cette approche examine les quatre problèmes suivants:

(1) L'évaluation de la configuration structurale et la chimie des interfaces étudiées par les méthodes d'analyses des interfaces internes, c'est-à-dire par MEHR et par spectroscopie de pertes d'énergie électronique à détecteur en configuration parallèle (SPEEP), en considérant les effects des différentes liaisons oxygène dans le système SiC-Si_3N_4.

(2) L'importance du rôle des impurités liées à la présence des whiskers, telles que du carbone et de l'oxygène en excès, sur la formation de la phase liquide et sur le développement de la microstructure du Si_3N_4 pur.

(3) La variété des microstructures locales, le long des joints de grains du composite Si_3N_4 renforcé par des whiskers, des plaquettes ou des fibres en SiC, due aux contraintes thermodynamiques qui augmentent la nature dynamique des internes dans les composites à matrice céramique, et enfin.

(4) Le problème fondamental de la corrélation des caractéristiques microscopiques des grains et des phases frontières avec le comportement à la rupture des matériaux composites, considérant que des paramètres macroscopiques, liés à la matrice influencent le comportement mécanique.

1 Introduction

In recent years a worldwide effort has been launched for oxide and nonoxide structural ceramics to overcome the barrier of brittle failure through either continuous fiber reinforcement or incorporation of SiC-whiskers, -platelets or -dispersoids. While the former concept has been proven successful, the latter failed after early optimistic hopes. Despite remarkable improvements in fracture toughness and strength distribution, ceramic composites employing discontinuous reinforcement components still undergo brittle failure.[1-5]

The structural configuration of interfacial boundaries as well as the chemical bonding state between the reinforcement component and the monolithic baseline material define a fundamental issue of composite research.

Due to the wide variety of interacting intrinsic and extrinsic parameters controlling both microstructure and mechanical response of composites, quantification of interfacial properties becomes difficult. Thus, interfacial boundaries are often classified in terms of being weak or strong. A weak interface is usually connected with an amorphous intergranular layer. This feature is prone to debonding and sliding close to the propagating crack which is generally appreciated for composites exhibiting high fracture toughness. In contrast, a strong interface is synonymous with direct bonding between the toughening component and the matrix. Although such boundaries may support crack deflection or load transfer, the composite material exhibits little or no improvement of fracture toughness because of whisker or fiber fracture.[6]

The real composite world, however, is only insufficiently described by such general models. Numerous experimental and theoretical approaches involving HREM studies of metal/ceramic systems, bicrystals and epitaxial growth of thin films as well as simulation of grain and phase boundaries[7-10] have provided quantitative bonding and geometrical models which contribute to a deeper understanding of internal interfaces in composites.

Since these interfaces define small two-dimensional defects on a nanometer scale, high-resolution electron microscopy (HREM) and high spatial resolution electron energy loss spectroscopy are necessary to evaluate their local chemistry and structural states, including segregation effects and chemical gradients between the constituents across the interfacial boundary. Such data provide valuable information which can be utilized as feedback for refinements of theoretical treatments of mechanical composite behavior.

In this context, the purpose of this paper is twofold. Firstly, the issue of oxygen segregation to whisker/matrix interfaces of SiC(w)/Si_3N_4 composites is discussed in the light of recent data obtained from parallel detection electron energy loss spectroscopy (PEELS) in conjunction with HREM studies of such boundaries. This approach includes a large variety of different commercial VLS-grown whisker raw materials and their effect on interfacial chemistry and microstructural development of both the monolithic baseline as well as the composite material. Moreover, the interaction of interfacial characteristics of grain and phase boundaries with the prevalent toughening mechanisms and the mechanical response of SiC/Si_3N_4 composites is discussed.

Secondly, the stability of the microstructure of SiC/Si_3N_4 composites is put into perspective, focusing on the internal stability of the constituents along SiC(w)/Si_3N_4 interfaces. Chemical degradation reactions and/or diffusion processes along

grain and phase boundaries can change the local phase composition at the interface or adjacent to it. Therefore, interfacial structures are emphasized as dynamic features which are controlled by the rules of thermodynamics, constraints from processing and raw materials as well as environmental conditions during service.

2 Materials and Instrumentation

VLS-grown SiC-whisker grades from four different sources (Tokai Carbon Ltd, Japan; Huber Inc., Borger, TX, USA; American Matrix Inc., Knoxville, TN, USA; Nikkei Ltd, Japan) produced during the 1986–1988 period are involved in this study. SiC-platelets were supplied by American Matrix Inc.

The Si_3N_4 baseline material was produced from Toyo Soda (Tosoh Corp., Tokyo, Japan) (TS 10) α-Si_3N_4 powder (1·5 wt% O; 0·07 wt% C; 0·03 wt% Cl; 0·01 wt% Fe) with a sintering additive composition of 5 wt% Y_2O_3 and 1·1 wt% Al_2O_3. Composites with 20 vol.% as-received SiC(w) were presintered at 1500°C in 0·1 MPa argon prior to encapsulation and HIPing. Complete densification was achieved by HIPing at 1780°C in 190 MPa argon. The same matrix material was utilized for processing SiC-platelet-based composites.

TEM foils were prepared by standard ceramographic techniques involving dimpling, Ar-ion beam milling using a cold-stage holder to avoid artifacts and carbon coating to reduce charging effects in the microscope.

HREM studies from interfacial boundaries were performed in an Akashi 002B (200 kV) microscope at the Arizona State University (ASU), Tempe, AZ, USA, utilizing a Scherzer resolution of 0·18 nm. A Philips EM 430 T TEM/STEM operating at 300 kV was used for conventional transmission electron microscopy including small probe microanalysis and convergent beam electron diffraction.

The chemistry at the interfacial boundaries was determined with a Philips 400 ST at ASU employing a field emission gun (FEG) operating at 100 kV. This microscope was attached to a parallel EELS detector (Gatan model 666) and a computer system to control the focused probe position. Coupling of the parallel EELS detector to the microscope was achieved in diffraction mode with an acceptance half angle of 10 mrad. A position-resolved PEELS technique was developed where the probe is stepped at preselected distance increments of 1 to 2 nm and a spectrum is collected at each position, thus utilizing a large amount of EELS data from a single boundary. A liquid nitrogen cooled specimen holder was used during small probe microanalysis to eliminate specimen-borne contamination. (It should be noted that the three axis/three index notation is adopted for hexagonal phases throughout this paper.)

3 Results and Discussion

This paragraph is organized into six sections. Sections 1–3 concern phases and interfaces in the two-phase stability field '$SiC + Si_3N_4$' of the Si–C–N–O system. The nature of disordered layers from $SiC(w)/Si_3N_4$ interfaces is discussed in the light of recent data obtained from HREM imaging and high-resolution PEELS. The issue of crystalline boundaries in ceramic matrix composites is addressed. Section 3.4 accounts for degradation reactions of the reinforcement component or environmental effects from processing which cause the nominal composite composition to shift outside the '$SiC + Si_3N_4$' stability field in the Si–C–N–O system. This introduces reaction products which not only influence interfacial properties but may also affect the densification of the baseline material. The morphological stability of SiC-whiskers exposed at high temperatures is discussed. Section 3.5 explores the effects of 'impure' reinforcement components on matrix grain growth and devitrification of the secondary phase and comments on failure-related defects in $SiC(w)/Si_3N_4$ composites. Section 3.6 addresses the interaction of interfacial structures and fracture resistance of $SiC(w)/Si_3N_4$ composites. Just how much of interfacial properties on a nanometer scale is reflected in the macroscopic mechanical response (fracture resistance) of a Si_3N_4-based composite, considering that matrix effects contribute to the prevalent toughening mechanism?

3.1 SiC-whiskers and -platelets: significance of bulk composition, surface morphology, structure for interfacial boundaries in $SiC(w)/Si_3N_4$ composites

SiC-whiskers and -platelets display a considerable variety of properties. Although the vast majority are certainly of importance for the general microstructure and the mechanical behavior of the densified composites, experience gained from studying SiC/Si_3N_4 composites has shown that bulk composition, surface morphology and the structure of as-received SiC reinforcement components are the most relevant properties for internal interfaces. Their significance will be outlined briefly in the following.

VLS-grown as-received β-SiC-whiskers contain a

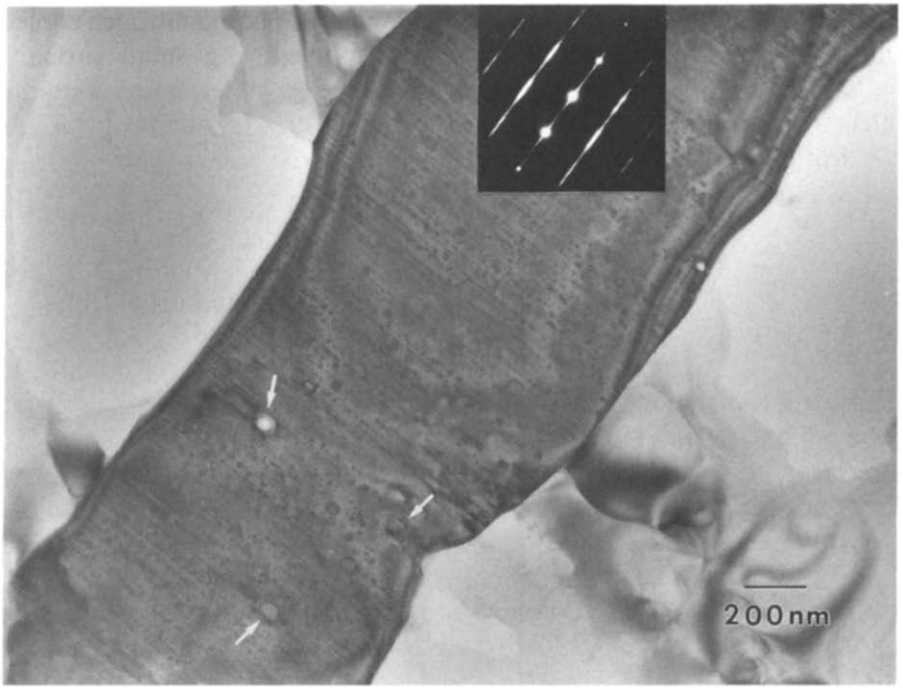

Fig. 1. SiC-whisker (American Matrix, 300 kV) in the [110] orientation with respect to electron beam. Note surface notches and numerous spherical inclusions (see arrows) attached to planar faults.

thin native surface layer which is enriched in excess carbon, oxygen and nitrogen translating into suboxides and silica-like species. These layers have been characterized by numerous surface analytical investigations by means of AES and XPS, accounting for the effects of whisker growth conditions and feedstock materials.[11-14] Usually β-SiC-whiskers contain a variety of metallic impurities, most of which are added in order to increase the whisker yield during processing.

It is important to note that most SiC-whiskers are not single-phase materials. Rice-hull derived SiC-whiskers, e.g. from Tateho, are well known for their characteristic low-density core region which provides a sink for the non-crystalline oxynitride phase in the consolidated Si_3N_4-based composite. Moreover, tiny spherical secondary-phase particles with average grain sizes of 10 nm were found to be dispersed throughout the bulk of some whisker grades, e.g. from American Matrix, where they are preferentially associated with stacking faults (Fig. 1). Similar features have been described for other SiC-whisker raw materials and identified as oxygen-rich, metal-bearing impurities[15] related to the VLS growth process.

These examples provide evidence that—besides the surface layer—additional sources of oxygen in SiC-whiskers must be considered. Therefore, the bulk chemistry rather than XPS data collected from a few monolayers of the whisker periphery probably provides a better judgement to account for shifts in the composite's nominal composition due to incorporation of non-stoichiometric, multiphase components like SiC-whiskers. Table 1 compiles the chemical bulk analysis of the whisker grades involved in this study, expressing them as components in the system Si–C–O–N. Calcium has been listed to account for the well-known detrimental effect of this network-modifying cation on the high-temperature strength of the Si_3N_4 baseline material and thus the composite.[17]

As in SiC-whiskers, most impurities in SiC-platelets are comparable to the levels established for average Si_3N_4 or SiC sintering powders. This is particularly true of the oxygen content. A recent chemical analysis of different SiC-platelet lots from American Matrix revealed oxygen up to 0·45 wt%, boron between 0·4 and 0·8 wt%, and aluminum up to 0·45 wt%.[18] The author's own analyses of platelets bought from the same supplier in 1989 resulted in

Table 1. Chemical analysis of as-received SiC-whisker grades from different sources. From Ref. 16

	Tokai Carbon	*Huber*	*American matrix*	*Nikkei*
C (wt%)	29·27	29·07	29·36	27·38
N	0·70	0·81	0·27	1·76
O	0·20	0·23	1·24	3·02
Si	69·6	69·8	68·9	67·4
Ca	0·01	0·01	0·15	0·21

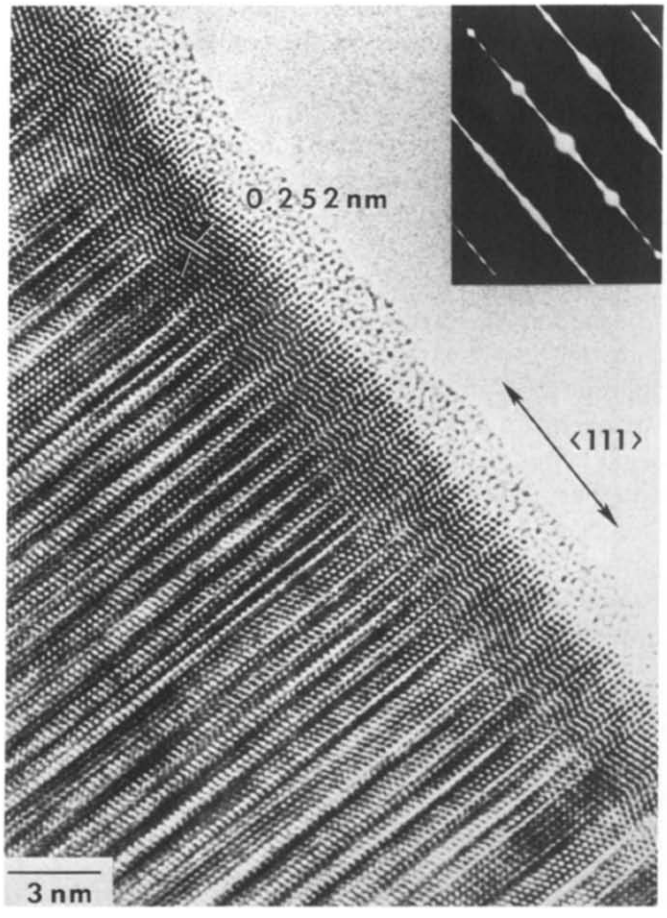

Fig. 2. HREM image (400 kV) of a β-SiC-whisker (Tokai Carbon) from SiC(w)/Si_3N_4 composite. Beam direction is parallel to [110]. The whisker is close to the edge of the foil; amorphous phase contrast is due to radiation damage during ion-beam thinning of the specimen. Note rough surface morphology due to microfacetting on {111} planes. Also note the high density of planar faults perpendicular to the [111] growth axis which give rise to intense streaking in the corresponding diffraction pattern (see inset). From Ref. 28.

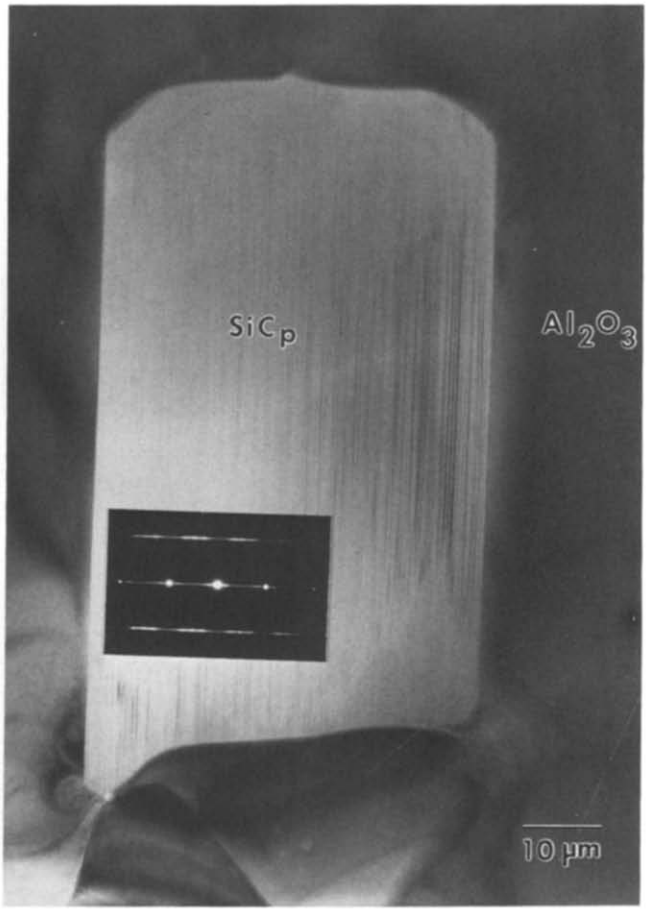

Fig. 3. SiC-platelet (American Matrix) embedded into a corundum matrix (300 kV). Orientation is parallel to [110]. Note smoothness of {001} basal planes and high density of planar faults.

0·48 wt% oxygen, 0·08 wt% nitrogen, 0·24 wt% aluminum and evidence of excess carbon.[19] Analytical data of recently developed SiC-platelet grades distributed through C-Axis Technology, Phoenix, AZ, USA report 0·66 wt% oxygen for the 'super-fine' grade (average grain size: 11 microns) and 0·14 wt% for the 'medium' grade (average grain size: 24 microns), respectively.[20]

The surface morphologies of SiC-whiskers and -platelets differ significantly. While β-SiC-whisker surfaces are rough on the atomic scale, due to microfaceting on {111} planes (Fig. 2), the basal plane surfaces of SiC-platelets are smooth and flat (Fig. 3). The surface topography defines an important feature because it can influence debonding and frictional sliding processes. The effect, however, depends on the dimensional scale. Whisker surfaces exhibiting roughness on an atomic scale may promote interlocking with fine-grained matrix constituents, while macroscopic notches may act as stress concentrators and strength-limiting flaws.[21] The smooth surfaces of SiC-platelets are ideally suited for crack deflection, particularly when the platelets are oriented parallel to the tensile stress axis.[5]

The significance of impurities during growth of α-SiC single crystals with platelet-like {001} morphology have been known at least since Knippenberg's[22,23] classic paper on growth phenomena in silicon carbide. A review of today's recipes for fabrication of SiC reinforcement components including platelets is given in Ref. 24.

The effect of aluminum is twofold: (i) the stabilization of 6H–SiC polytype (Fig. 4) as the dominant polytype besides 4H and 15R, and (ii) as a surface reacting agent in combination with boron in order to promote growth of {001} basal planes by simultaneously reducing the growth rate parallel to the c-axis.

SiC-whiskers and -platelets exhibit a high density of planar faults making it very difficult to address a single well-defined polytype (Figs 2 and 3). In such

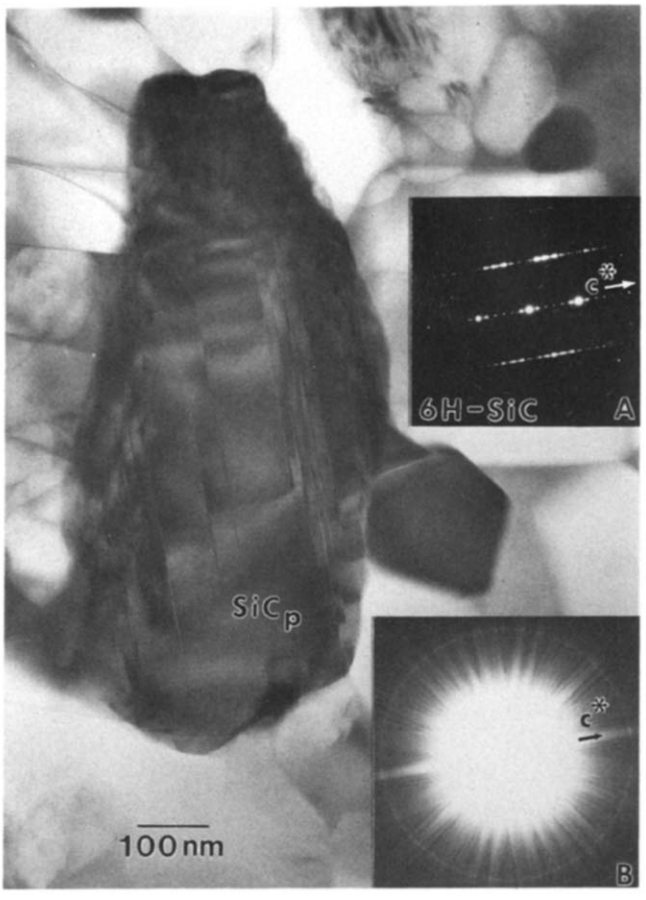

Fig. 4. SiC-platelet (American Matrix) from Si_3N_4-based composite (beam direction is parallel to [110], 300 kV). 6H–SiC polytype is revealed from stacking sequence down the c^*-axis in reciprocal space due to extra (kinematically forbidden) reflections between the central beam (000) and the (006) Bragg spot. Inset B is a large-angle CBED pattern obtained with a low camera length setting taken from the same location as SAD pattern A. The diameter of the FOLZ-ring displayed is consistent with the 6H–SiC polytype. From Ref. 19.

cases the structural configuration is best described as a random mixture of short-period SiC polytypes.[25]

3.2 HREM and EELS nanospectroscopy of SiC(w)/Si_3N_4 boundaries: evidence for discontinuous oxygen distribution

In the SiC(w)/Si_3N_4 system oxygen is supplied from the Si_3N_4 starting powder and the SiC-whiskers, as well as from sintering aids, and is distributed along the grain boundary network during liquid-phase assisted sintering of the composite. Thus, a significant amount of oxygen segregation to internal interfaces is expected.

Grain and phase boundaries from several SiC(w)/Si_3N_4 composites have been investigated by TEM.[26,27] While a study of a Tokai Carbon SiC(w)/Si_3N_4 material showed that discontinuous amorphous layers exist at whisker/matrix interfaces and that oxygen could not be detected at fully crystalline interfaces by serial EELS,[28] other HREM observations led to emphasis on the continuous nature of thin glassy films at SiC(w)/Si_3N_4 interfaces.[29]

HREM imaging and EELS interface analysis of SiC(w)/Si_3N_4 boundaries include intrinsic and instrumental constraints which merit a short comment in terms of the different resolution limits involved. As discussed in more detail in Ref. 30, spatial resolution is basically limited by the current density in the focused probe, the collection time for an EELS spectrum, radiation effects and the temporal stability of the probe/specimen. For challenging objects like interfacial structures the spatial resolution limit should be as close as possible to the interpretable image resolution limit which, for most of today's microscopes, is in the 0·14 to 0·18 nm range. Spatial resolution of the serial EELS experiments from Ref. 28, however, was limited by specimen and stage drift during the rather long collection time of the EELS spectrometer (100 s). Even with a field-emission electron source, it was in the order of 5 nm. When a parallel ELS detection system[31,32] became available soon thereafter, the collection time was reduced by a factor of between 500 and 1000, which drastically improved spatial resolution and offered capabilities for true nanospectroscopy on a 2 nm scale of spatial resolution.[33]

Oxygen segregation at interfacial boundaries in SiC(w)/Si_3N_4 composites was investigated by combining interface analysis with the FEG/PEELS system and HREM studies. Four β-SiC-whisker grades (see Section 2) with different amounts and types of impurities were employed in this study. These investigations revealed some fundamental aspects between interfacial chemistry and type of bonding which hold for all whisker raw materials investigated. A comprehensive discussion of this issue is given elsewhere.[34–36] The results can be summarized briefly as follows:

(a) A continuous, oxygen-rich, nitrogen-depleted amorphous layer was established at matrix grain boundaries, which is in agreement with the current understanding of a continuous oxynitride amorphous phase at most grain boundaries from liquid-phase sintered Si_3N_4 materials.[37–39]

(b) Discontinuous oxygen-rich disordered (amorphous) regions were observed at whisker/matrix interfaces, thus confirming earlier findings obtained by serial EELS.[28] Crystalline regions exhibiting direct bonding between SiC-whiskers and β-Si_3N_4 were identified in these materials. Amorphous and crystalline

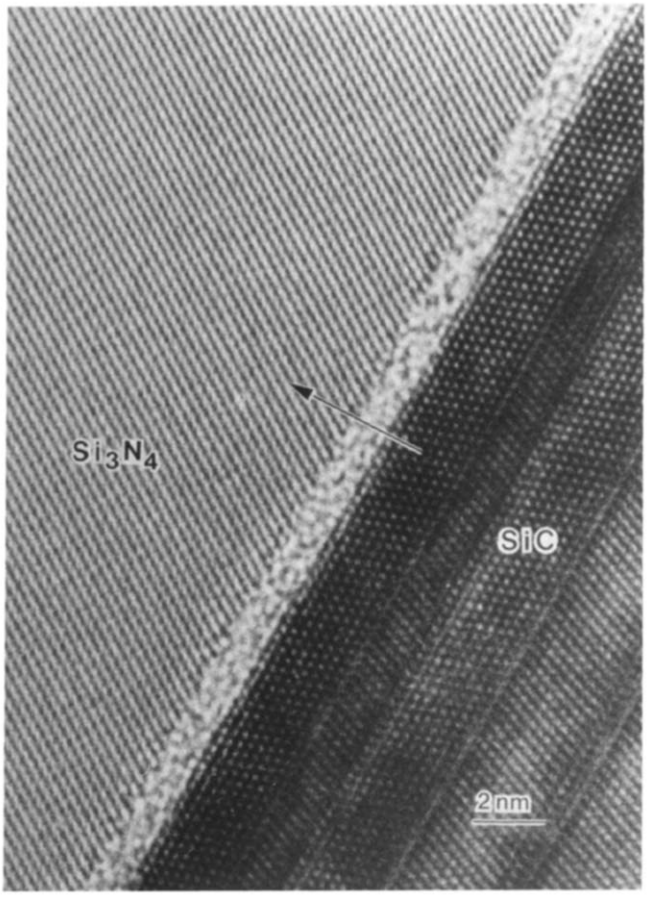

Fig. 5. HREM image (200 kV) of Huber SiC(w)/Si_3N_4 interfacial boundary. The interface is viewed edge-on with the β-Si_3N_4 grain in $g = \langle 001 \rangle$ two-beam conditions and the β-SiC oriented parallel to [110]. The scan path of the focused probe (see Fig. 7) is indicated by the arrow. The interface clearly reveals an amorphous interlayer. The structural width is of the order of 1·5 to 2·0 nm. From Ref. 36.

regions may even occur periodically at the same interface, as shown in the HREM images of Figs 5 and 6. The corresponding oxygen distributions obtained by position-resolved PEELS are depicted in Figs 7 and 8. The HREM image in Fig. 5 reveals a thin amorphous layer at the interfacial boundary. In the digital EELS scan (Fig. 7) the integrated oxygen *K*-edge intensity displayed as a function of the distance across the interface rises sharply at the interface adjacent to the SiC-whisker and then drops off to higher background level in the β-Si_3N_4 grain relative to the oxygen level in the SiC-whisker.

Figure 6 shows an HREM image obtained from the same boundary, taken approximately 20 nm away from the amorphous region displayed in Fig. 5. Note the absence of a visible amorphous layer at the interface and almost perfect direct bonding with no moire-fringes between the β-SiC-whisker and the β-Si_3N_4 matrix grain. This different interfacial structure is clearly monitored in the digital EELS scan (Fig. 8). No sharp increase in oxygen concentration is recorded, only a constant and high oxygen level in the β-Si_3N_4 grain, similar to the situation shown in Fig. 7.

(c) It is important to note the large difference between the structural interface width as determined from HREM images and the chemical interface width as determined from

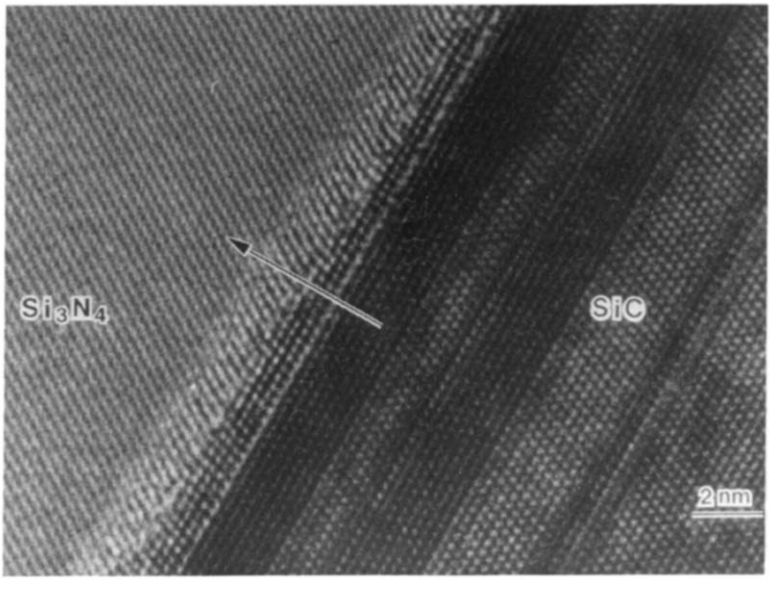

Fig. 6. HREM image (200 kV) of the same interfacial boundary displayed in Fig. 5, taken approximately 20 nm away from the region shown in Fig. 5. The image reveals direct bonding between the whisker and the β-Si_3N_4 matrix grain with no indication of amorphous phase present. Orientation of constituents corresponds to Fig. 5. The scan path of the focused probe (see Fig. 8) is indicated by the arrow. From Ref. 36.

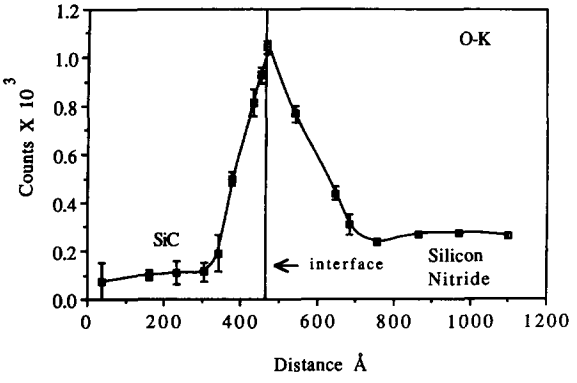

Fig. 7. Variation of oxygen concentration obtained by PEELS as a function of distance from the whisker/matrix boundary including an amorphous interlayer as shown in Fig. 5. Note the sharp fluctuation in oxygen concentration at the interface and the wide difference in the structural and chemical widths of the interface. Again note the high oxygen background in the β-Si_3N_4 grain. From Ref. 36.

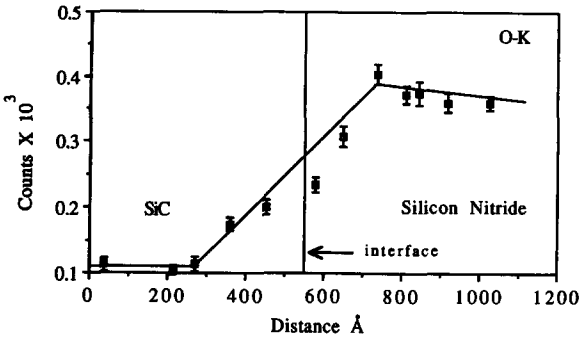

Fig. 8. Variation of oxygen concentration obtained by PEELS as a function of distance from the directly bonded whisker/matrix interface as shown in Fig. 6. No sharp fluctuation in oxygen concentration is detected at the interface. Note the difference in chemical and structural widths of the interface. Also note the high oxygen concentration in the β-Si_3N_4 matrix grain region compared to the β-SiC. From Ref. 36.

the oxygen distribution by means of PEELS. The structural width is usually of the order of 1·5 to 2 nm. The chemical width is dominated by the β-Si_3N_4 matrix grain and is 20–30 nm on average. Not surprisingly, the chemical width for a β-Si_3N_4/β-Si_3N_4 boundary of the baseline material was found to increase by a factor of two compared to a SiC(w)/Si_3N_4-type of boundary.[35] The relatively high oxygen level in the matrix grain is attributed to dissolution of oxygen from the Y- and Al-bearing non-crystalline oxynitride phase in the β-Si_3N_4 matrix grains, following schematically a β'-sialon-type $Si_{6-x}Al_xO_xN_{8-x}$ substitution mechanism to maintain charge neutrality. Due to the limited aluminum content of the starting batch the extent of the substitution reaction given by the parameter x, however, is believed to be very small. The actual chemical width of the interfacial boundary will therefore depend on (i) concentration gradients of the constituents between the interface and the matrix grain, and (ii) the time and temperature allowed for diffusion across the boundary.

(d) Besides these interfacial characteristics shared by all SiC(w)/Si_3N_4 composites investigated, principal differences in interfacial roughness and both periodicity and lateral widths of amorphous and crystalline regions along interfacial boundaries were observed.[36] These observations, along with the PEELS/HREM results already discussed, strongly suggest that interfacial properties, e.g. bond and shear strengths and elastic parameters depend on the position in the interfacial boundary and rarely match the requirements of continuum mechanics models.

It is particularly the interaction of a propagating crack with the periodic patterns of amorphous and crystalline regions along a whisker/matrix boundary which will have to be explored in the future.

The crystalline regions observed at SiC(w)/Si_3N_4 boundaries are an interesting result. Direct bonding of constituents is by far not uncommon in ceramic materials. SiC/SiC epitaxial interfaces from reaction-bonded SiC materials are a good example for a crystalline, presumably 'strong' boundary in monolithic structural ceramics.[40] Crystalline interfaces have also been reported from SiC(w)/Al_2O_3 materials[28] and nanocomposites.[41] TEM studies from bicrystals and thin films indicate that most crystalline interfacial boundaries are supported by orientation relationships.[42] It is believed that this is also true for β-SiC(w)/β-Si_3N_4 boundaries. Work is now in progress to characterize these crystalline regions in more detail.

Very few HREM studies have been performed on interfacial boundaries in SiC(platelet)-based composites. Thick amorphous films have been reported for SiC(platelet)/Al_2O_3 boundaries.[43] No PEELS experiment focusing on interfacial chemistry similar to the approach already discussed had been published at the time of writing this paper. Considering the interest SiC-platelet reinforcement has raised in the ceramic community, more HREM studies and microanalytical investigations are expected to be published in the future.

3.3 How much of the whisker-related oxygen is monitored by PEELS at interfacial SiC(w)/Si_3N_4 boundaries?

The chemical width of SiC(w)/Si_3N_4 boundaries as revealed from the position-resolved PEELS data defines an intrinsic composite feature which is controlled by different sources of oxygen. Such sources are the sintering aids and the surface impurities from both the SiC-whiskers and the α-Si_3N_4 starting powder. A comparison of the chemical widths at whisker/matrix interfaces versus the oxygen content of the as-received whisker grades did not reveal a consistent correlation. That is, no significant difference was evaluated between the extremes, e.g. the 'low-impurity' Tokai Carbon and the 'high-impurity' Nikkei batches (compare with Table 1) respectively.[36]

This finding is not surprising. By sheer quantity the effect of oxygen supplied via sintering aids and Si_3N_4 starting powder will dominate over the effects of surface contaminants from the whisker raw material. The oxygen-rich surface layer of the as-received SiC-whiskers will certainly increase the local amount of liquid phase in the SiC(w)/Si_3N_4 compact. But considering the basic mechanisms of liquid-phase sintering in the Si_3N_4 system, this very fraction of liquid phase will not stay where it originated but will rather be distributed throughout the grain boundary network due to particle rearrangement, capillary forces and diffusion processes. As a consequence, it is virtually impossible to discriminate oxygen supplied from sintering aids versus oxygen derived from whisker surface contaminants at an arbitrarily chosen interfacial boundary in the microstructure. Thus, in conclusion, it is an integral effect of different sources of oxygen which contributes to the chemical widths observed at SiC(w)/Si_3N_4 interfaces.

This finding is valid for systems which follow a liquid-phase sintering process, but it may not be true for ceramic matrices such as Al_2O_3 which are controlled by solid-state sintering.

For a SiC(w)/Al_2O_3 composite material, the following rationale correlating the whisker surface chemistry with both fracture mode and fracture toughness has been derived:[44,45] fracture surface compositions involving Si–O–C species, free carbon and/or hydrocarbons result in an intergranular fracture mode, a presumably weak whisker/matrix bond and a high fracture toughness, while rather clean surfaces or such exhibiting Si_2N_2O or SiO_2 species were related to transgranular fracture mode, a presumably strong whisker/matrix bond and thus low fracture toughness. These findings were interpreted as an effect of the whisker surface species on the structure/composition of the whisker/matrix interface and thus on fracture mode and crack propagation.

It should, however, be emphasized that surface contaminants and impurities related to the reinforcement component may influence grain growth and general microstructure of the matrix material which nevertheless translate into the different mechanical responses to the composite (see also Section 3.5).

3.4 Interfacial reactions at SiC/Si_3N_4 boundaries due to degradation of the reinforcement component (whiskers, platelets, fibers) and environmental effects

The microstructure along interfacial boundaries in SiC/Si_3N_4 composites is a very sensitive tool for monitoring degradation reactions of reinforcement components or even local fluctuations of phase equilibria. As reaction products affect interfacial properties, their evaluation defines an important characterization task. Particularly the graphite formation along interfacial boundary will be addressed later in this section.

Although phase assemblages of fine-grained structural ceramics rarely represent conditions close to thermodynamic equilibrium, phase equilibria studies in the Si–C–N–O and related systems[46,47] nevertheless furnish valuable background information on which reaction schemes are to be expected at SiC/Si_3N_4 boundaries. The key point to consider for this approach are the boundary conditions for the two-phase '$SiC + Si_3N_4$' stability field which are basically defined by the thermal decomposition reaction of Si_3N_4 and the SiC nitridation reaction. The corresponding processing window requires stringent conditions with respect to the nitrogen partial pressure and the sintering temperature.[48]

Focusing on the issue of graphite, a comparison of different Si_3N_4-based composites reveals that graphite is indeed a common interfacial reaction product irrespective of the type of SiC reinforcement component employed. Although the local microstructures at the boundaries from whisker-, platelet- and continuous fiber- (Nicalon) reinforced materials look very similar (compare Figs 9, 10 and 11), graphite formation is believed to result from different mechanisms which are discussed briefly in the following outline:

(i) The in-situ decomposition reaction of a SiC-whisker involving graphite formation is demonstrated in Fig. 9. This Si_3N_4-based composite was processed under high nitrogen pressure on purpose, thus leading to

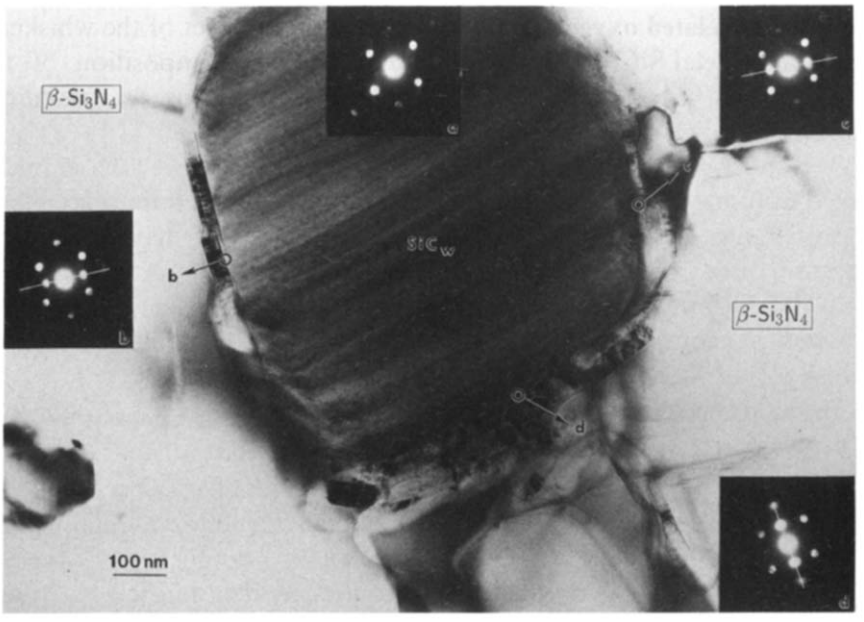

Fig. 9. Graphite formation along the interfacial boundary between a SiC-whisker (Tokai Carbon) and the Si_3N_4 matrix due to chemical degradation of the whisker during a presintering treatment of the composite in nitrogen atmosphere (300 kV). CBED patterns inserted consist of {002} graphite reflections superimposed on an α-SiC ($B=[-\bar{6}\ -\bar{3}\ 1]$) pattern. Image and CBEDs reveal an almost continuous graphite layer along the whisker periphery.

nitridation of the SiC-whisker and formation of graphite according to the reaction

$$3SiC(s) + 2N_2(g) \rightarrow Si_3N_4(s) + 3C(s)$$

(ii) Graphite formation at interfacial boundaries is observed also in an as-sintered SiC-platelet-reinforced Si_3N_4 material (Fig. 10). Appropriate reaction schemes can be derived from phase equilibria studies and it is quite interesting to include interfacial reactions from a Nicalon fiber (see Fig. 11), because, like whiskers and platelets, Nicalon is a non-stoichiometric SiC reinforcement component containing oxygen and excess carbon.[49]

Greil[50] has recently calculated degradation schemes of Si–C–O components in argon atmosphere in the temperature range of 1000°C to 2000°C. Oxygen-containing reinforcement components start to decompose at temperatures of the order of 1000°C, releasing gaseous species like SiO and CO. In SiC components containing free carbon, such as whiskers, platelets and fibers, CO is the dominating species following

$$3C(s) + SiO_2 \rightarrow SiC + 2CO(g)$$

At even higher temperatures SiO evaporation occurs according to

$$SiC(s) + SiO_2(s) \rightarrow C(s) + 2SiO(g)$$

This latter reaction scheme is believed to account at least for the graphite formation observed in the Nicalon-SiC-fiber/Si_3N_4 composite (Fig. 11) which was hot-pressed at 1750°C/30 MPa argon atmosphere. It is interesting to note that the SiO was identified as the dominating gaseous species by mass-spectroscopic vapor pressure studies during annealing of Nicalon fibers.[51]

Graphite formation along SiC(platelet)/Si_3N_4 boundaries (Fig. 10), however, seems to be related to excess carbon enriched on the SiC-platelet surface. A chemical degradation reaction appears to be of secondary importance because graphite was also observed for composite batches which utilized SiC-platelets pretreated with HF.[19]

Schoenlein *et al.*[52] report a very similar microstructure as displayed in Fig. 11 for a Nicalon fiber-reinforced hot-pressed silicon nitride material. MgO was employed as sintering aid and the compact was processed at 1750°C in nitrogen atmosphere. The occurrence of a graphite layer adjacent to the Nicalon fiber is, however, explained by an in-situ formation during fabrication, due to exsolution of excess carbon from the fiber.

(iii) Graphite-rich interfacial reaction layers have also been reported from Nicalon-SiC-fiber-reinforced glass–ceramic systems.[53] Graphite formation in oxide matrices such as glass–ceramic systems follows different rules than discussed previously for the Si_3N_4-based composite of the present study. As shown by

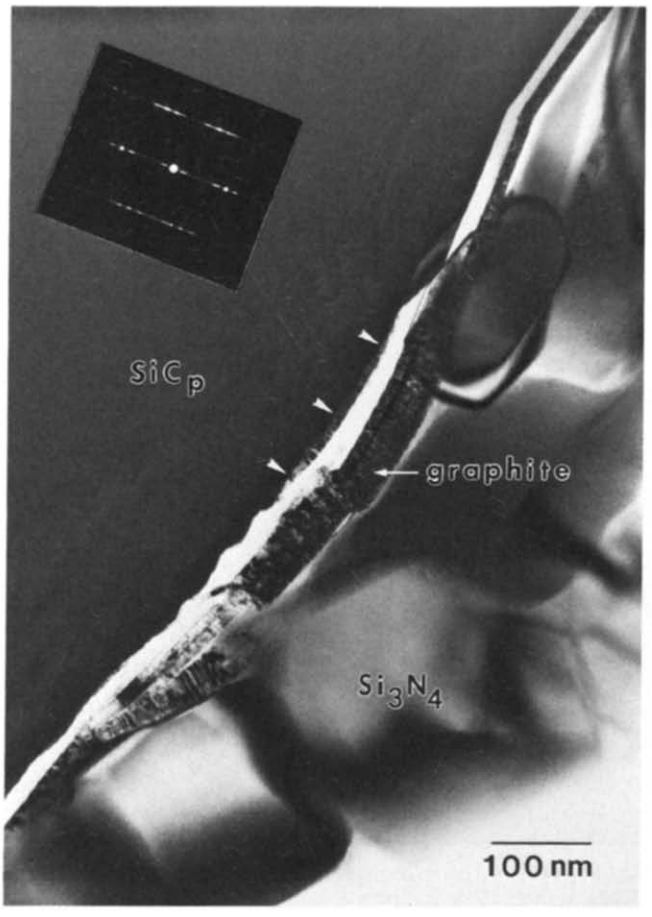

Fig. 10. Graphite layer at the interfacial boundary of a SiC-platelet (American Matrix) and the β-Si_3N_4 matrix (300 kV) in as-sintered Si_3N_4-based composite. From Ref. 19.

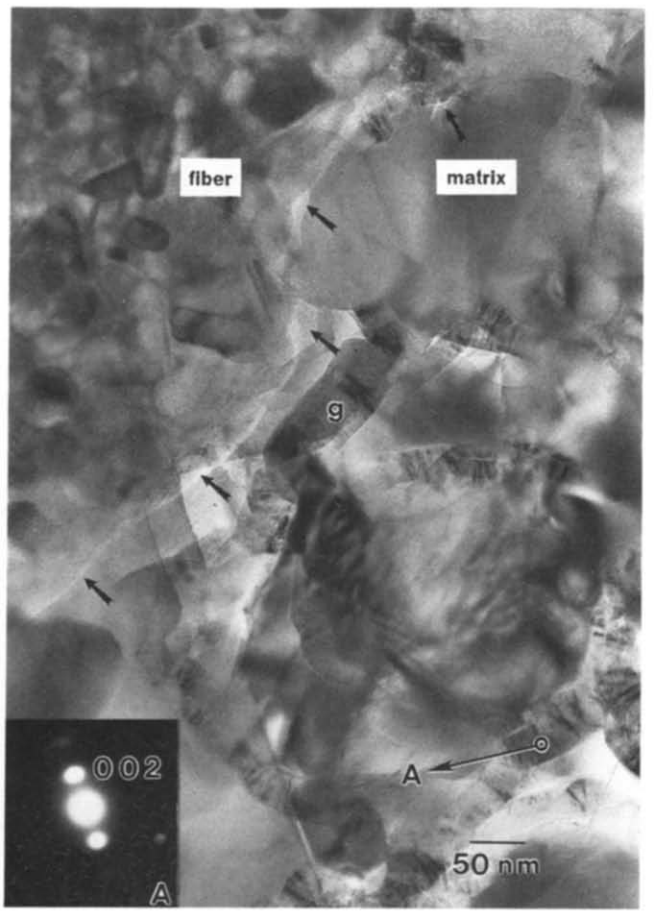

Fig. 11. Interfacial area in hot-pressed Nicalon–SiC(fiber)/Si_3N_4 composite (300 kV). The fiber consists of fine-grained, recrystallized α-SiC crystals, separated from the matrix by a very fine-grained amorphous, presumably carbon-rich phase. The irregular lineament marked by arrows is interpreted as the fiber/matrix boundary which seems to hold a considerable amount of micropores. This boundary appears more clearly for negative defocus settings. Somewhat displaced from the boundary, typical ribbon-like turbostratic graphite crystals are dispersed throughout the β-Si_3N_4 matrix. Inset A displays a CBED with {002} graphite Bragg reflections from location A.

Cooper & Chyung,[54] graphite formation is due to an SiC oxidation reaction

$$SiC(s) + O_2(g) \rightarrow SiO_2(s) + C(s)$$

with the gradient in silica activity between the fiber and the matrix acting as the driving force behind the reaction.

Besides reaction schemes along interfacial boundaries involving graphite formation, there is evidence that the local microstructure is affected by other mechanisms.

The presence of excess silica due to the amorphous oxynitride grain boundary phase in SiC(w)/Si_3N_4 composites may lead to decomposition of SiC following the reaction

$$3SiC(s) + 3SiO_2(s) + 2N_2(g) \rightarrow Si_3N_4(s) + 3SiO(g) + 3CO(g)$$

It is believed that this decomposition reaction provides the nitrogen source for thin β-Si_3N_4 films grown epitaxially on β-Si_3N_4 matrix grain facets which are occasionally observed in SiC(w)/Si_3N_4 composites (Figs 12 and 13). As these materials represent stable two-phase '$SiC + Si_3N_4$' assemblages, this observation obviously reflects local chemical gradients or fluctuations in phase equilibria.

Whether a degradation reaction releasing SiO and/or CO species becomes critical with respect to the internal stability of a SiC reinforcement component also depends on the service conditions of the composite, as pointed out by Luthra.[55] If exposed to an inert atmosphere like argon, SiO and/or CO can migrate away from the interface, thus enhancing thermal decomposition and lowering the thermal stability of a SiC-based reinforcement component. Migration of gaseous species is supported by the fact that SiC(w)/Si_3N_4 composites exhibit considerable residual tensile stresses.[56] They can promote debonding of reinforcement components and generation of microcracks which would help gaseous

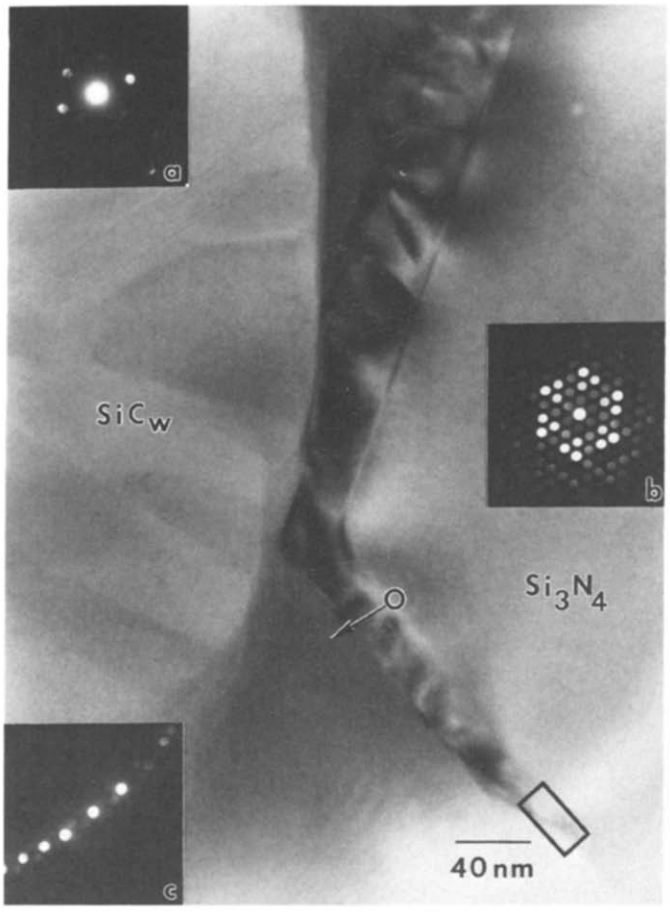

Fig. 12. SiC-Whisker (Tokai Carbon) with smoothly curved surface adjacent to a β-Si_3N_4 grain in close contact in SiC(w)/Si_3N_4 composite (300 kV). Note layer-like structure covering a {100} β-Si_3N_4 facet. Insets a, b and c refer to CBED patterns from the α-SiC-whisker (B = [001]), the β-Si_3N_4 (close to B = [001]) and the boundary adjacent to the layer structure. For enlargement of boxed area see Fig. 13.

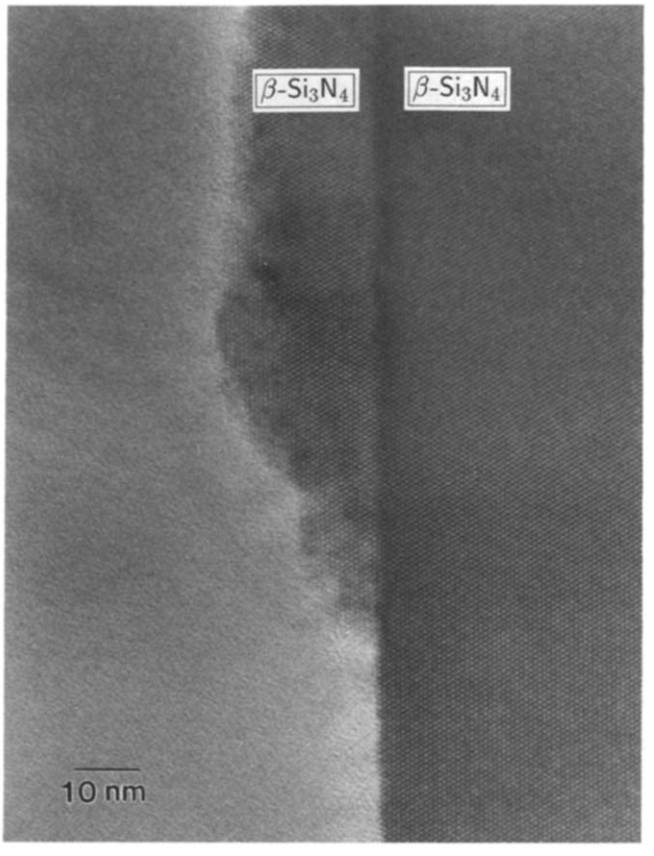

Fig. 13. β-Si_3N_4 layer grown epitaxially on {100} facets of β-Si_3N_4 matrix grain (300 kV, enlargement from Fig. 12). Orientation of both β-Si_3N_4 generations is parallel to [001].

species to escape from the local microstructure. Moreover, the grain boundary diffusion coefficient of carbon is in the order of 10^{-5} to 10^{-6} cm^2/s at high temperatures,[57] indicating that SiC/Si_3N_4 interfaces indeed act as a fast diffusion path. Possible evidence for CO migration along internal interfaces comes from microcrystalline graphite filaments dispersed at Al_2O_3 matrix triple-grain junctions in a SiC(w)/Al_2O_3 composite.[28] Most likely graphite is formed after condensation of a carbon-rich vapor phase accidentally trapped in a glassy-phase pocket, although nucleation from an oxycarbide liquid cannot be ruled out.

Interfacial reaction products heavily affect the mechanical response of composites. This is particularly true for graphite or graphitized carbons from continuous fiber-reinforced materials. They act as a solid lubricant which greatly improve interfacial properties. Their laminar structure provides a perfect weak bond at the interfacial boundary, thus promoting debonding and increasing fracture resistance. Strong enough to achieve load transfer into the stiffer fiber, they can accumulate a certain amount of local damage before they eventually fail prior to the fiber.[6,49]

3.4.1 On the morphological stability of SiC-whiskers at high temperatures

The aspect ratio of as-received SiC-whisker grades is a critical parameter[1,4,21] for effective toughening, which has to be preserved during the processing route of the composite as far as possible.

The morphology of SiC-whiskers, however, can change after prolonged exposure at high temperatures (Fig. 14). The corresponding Si_3N_4-based composite contained a total of 15 wt% sintering additives and was densified during gas-pressure sintering at 5 bar nitrogen/1975°C. SiC-whiskers in the as-sintered compacts consist of α-SiC. Although the majority of the whiskers incorporated appeared to be unharmed, a striking globularization and reduction in grain size was noticed for the other fraction.

A similar observation—however, from a single-phase SiC system—has been reported after annealing VLS β-SiC whiskers in a graphite furnace at

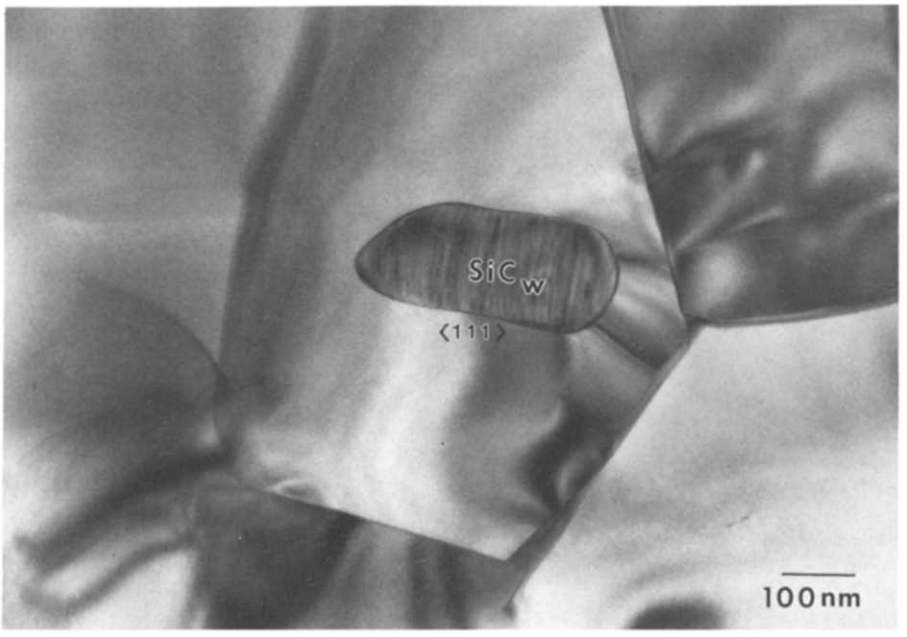

Fig. 14. Prolonged high-temperature exposure of SiC(w)/Si_3N_4 composites may enhance globurization of SiC-whiskers (300 kV). Compared to as-received whiskers, this process is characterized by smoothening of whisker ends and a reduction in grain size which may bind the whisker intragranularly to β-Si_3N_4 matrix grains.

1900°C and 2000°C in Ar atmosphere.[59] The whiskers became spherical with silicon-depleted envelopes left at the whisker ends. The shape change was accompanied by a beta-→alpha-SiC phase transformation which was probably assisted by some degradation reaction releasing SiO, as discussed in Section 3.4.

Shape changes of reinforcement components initiated by surface energy changes at high temperatures are emphasized by Luthra.[55] Because of their small grain sizes, SiC-whiskers are very susceptible to surface energy related effects such as Ostwald ripening. Morever, needle-like growth of β-SiC-whiskers requires a very delicate optimization of VLS process parameters, such as the substrate temperature, the C/Si ratio in the gas mix and the silicon supersaturation.[60] Therefore it is anticipated that the elongated morphology of SiC-whiskers characterized by a high aspect ratio is in fact metastable. In the case of inappropriate annealing conditions assisted by thermal degradation reactions, phase transformations and/or changes in surface energy, SiC-whiskers will approach an equiaxed equilibrium grain morphology similar to shape changes observed during high-temperature annealing of SiC-powders.[61]

3.5 Matrix effects related to densification behavior, phase composition and fracture strength of SiC(w)/Si_3N_4 composites

It has been emphasized in Section 3.1 that SiC reinforcement components contain a significant amount of free carbon and oxygen. Particularly the liquid-phase formation process in the Si_3N_4 system is strongly influenced by these impurities.

Because of CO evaporation carbon reduces the nominal additive concentration, resulting in a reduction of liquid-phase formation. The alpha/beta-Si_3N_4 phase transformation is retarded or even incomplete, which favors a more globular instead of elongated matrix grain growth.[62] These constraints require major adjustments in the processing routine for the composites and they were observed for whisker- and platelet-reinforced Si_3N_4 materials.[63]

Oxygen added to the Si_3N_4 baseline material can cause the nominal bulk composition to shift, thus introducing new phase assemblages. This has recently been verified by comparing the secondary phase assemblages from SiC-platelet-reinforced Si_3N_4 materials employing different platelet purity:[19] incorporation of as-received SiC-platelets results in partial devitrification of the amorphous phase at triple-grain junctions of the matrix, yielding $Y_2Si_2O_7$ polymorphs. Reducing the oxygen content of as-received platelets by an HF treatment did not cause the amorphous secondary phase to devitrify. The composite material exhibiting partial devitrification showed improved high-temperature deformation characteristics which is, however, due to a matrix effect and not because of platelet/matrix interaction.

The matrix contribution to fracture resistance of Si_3N_4-based composites is primarily controlled by the aspect ratio and the diameter of the elongated β-

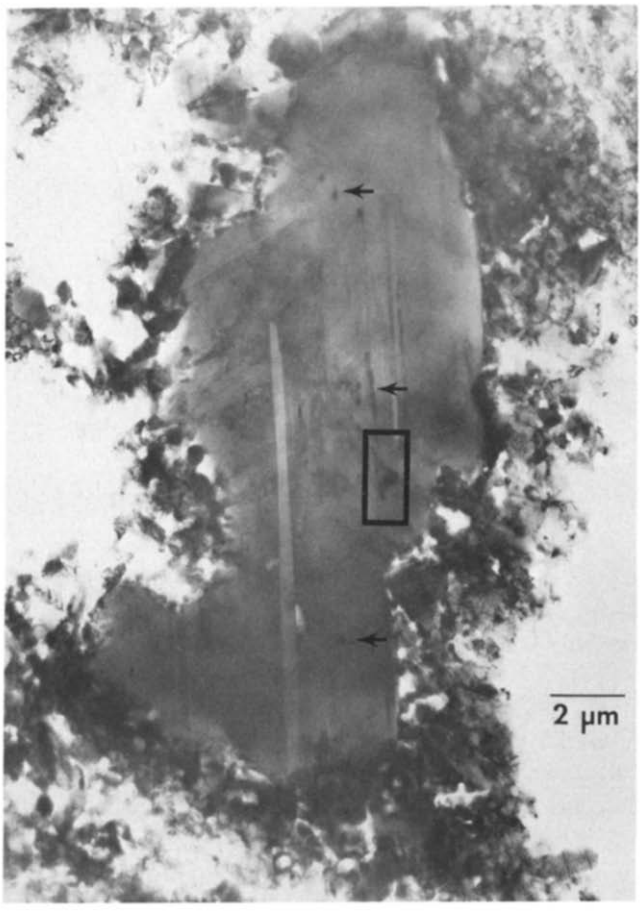

Fig. 15. SiC-whisker (Tokai Carbon) of unusual large grain size in SiC(w)/Si_3N_4 composite (300 kV), revealing crystalline secondary phase particles associated with stacking faults (see arrows). Small probe microanalysis (EDS) of the boxed region showed enrichment of zirconium which presumably translates into a Zr-silicide. Zirconium was probably employed to increase the whisker yield during the VLS process. From Ref. 67.

Si_3N_4 matrix grains, resulting in remarkable fracture toughnesses.[4,21] Thus, the influence of nominal additive composition and the processing conditions on the morphology of β-Si_3N_4 matrix grains is probably the most important aspect to consider in this context.[64]

Although this outline is focusing on the Si_3N_4 system, it is important to notice that similar constraints hold for alumina too. Chemical inhomogeneities in the alumina system, particularly excess calcium and silicon, alter the grain size distribution and facilitate discontinuous grain growth[65] or give rise to local liquid-phase formation.[66] Increasing the matrix grain size enhances toughnesses of both matrix and composites.[45]

A careful analysis of fracture surfaces from SiC(w)/Si_3N_4 composites indicates that whisker-related impurities are of minor significance for the room-temperature fracture strength of these materials.[67] Some interesting microstructural features relating whisker impurities to the particular VLS growth process have been revealed (Fig. 15). However, such impurities did not correlate with critical flaws in SiC(w)/Si_3N_4 composites such as machining defects, whisker-free microstructural heterogeneities and exaggerated grain growth of β-Si_3N_4 matrix grains (Fig. 16). The critical flaw size is usually of the order of 150 microns, as indicated by an estimate based on the Griffith approach. The critical parameters affecting homogeneity of the as-sintered microstructure and thus fracture strength of the composites are the morphology and the size of the whiskers employed.

3.6 Interfacial structures and fracture resistance of SiC(w)/Si_3N_4 composites

While fracture strength of SiC(w)/Si_3N_4 composites is controlled by macroscopic features several orders of magnitude beyond the scale of interfacial effects, fracture resistance is directly addressed to variations of interfacial structures. This issue has been investigated by HREM and analytical electron microscopy.[26] Usually, however, even different whisker grades added to a composite at a constant amount translate to a very similar increase in fracture toughness. This was also observed for the SiC(w)/Si_3N_4 from this study, resulting in a relative increase of approximately 30% in K_{IC}.[67]

It is believed that the structural configurations of interfacial boundaries, as discussed in Section 3.2, account for this improvement in fracture toughness. For the Si_3N_4 system, however, the accurate correlation of composite response to microscopic (interfacial) features is not easily achieved because of macroscopic, matrix-related contributions—such as grain size and grain shape—to the overall fracture resistance of the composite. Moreover, microscopic and macroscopic constraints interact in a complex manner.

This will be discussed in more detail after briefly reviewing the role of interfacial boundaries in the prevalent toughening mechanisms of SiC(w)/Si_3N_4 systems.

In composites with discontinuous reinforcement components, a number of toughening mechanisms involving crack bridging, crack deflection and stress-induced microcracking have been identified and rationalized in theoretical failure models.[68-72] Unlike continuous fiber-reinforced ceramic matrices, the effect of pull-out in SiC(w)/Si_3N_4 composites with low whisker content is considered very small.[4,21] While in fiber-reinforced composites pull-out is the predominant toughening mechanism which directly utilizes the structure/properties relationship of the interfacial boundary,[73-75] crack

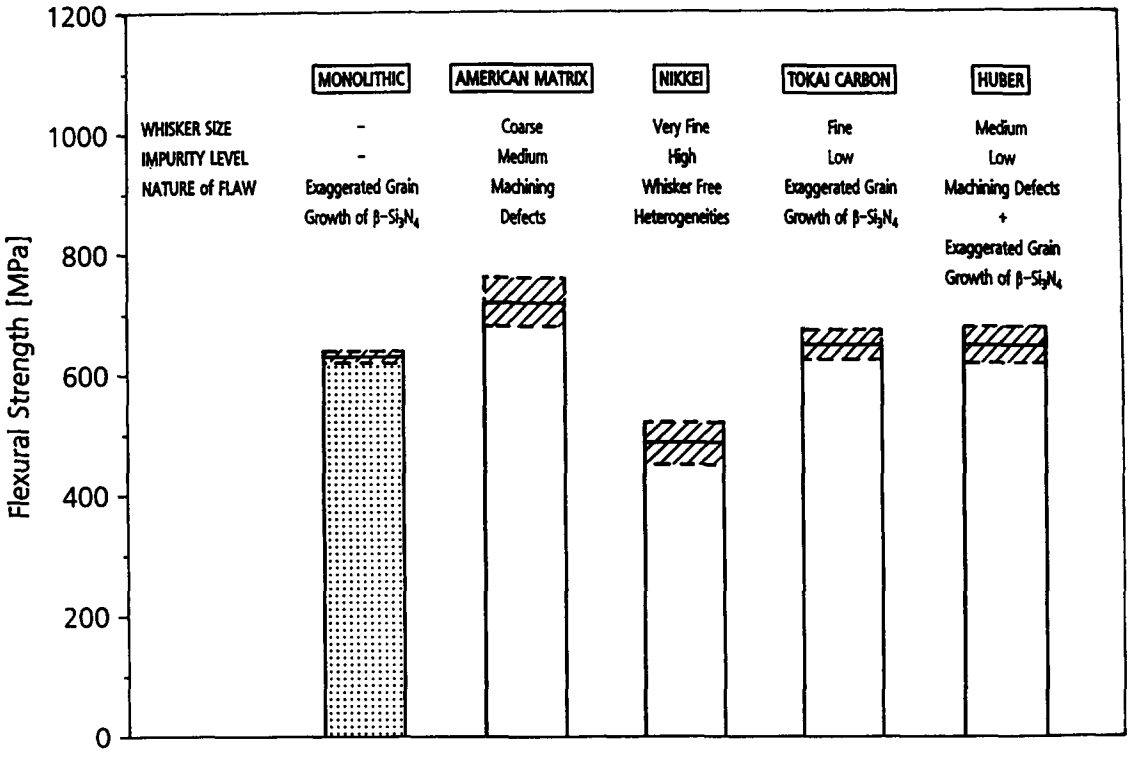

Fig. 16. A comparison of room temperature flexural strength of SiC(w)/Si_3N_4 composites employing SiC-whiskers from different sources and Si_3N_4 baseline material. From Ref. 67. The different whisker raw materials are characterized in terms of whisker size and impurity level. The nature of failure-related flaws was determined by fractography.

propagation in SiC(w)/Si_3N_4 composites follows a different toughening mechanism where fracture resistance for the most part is controlled by matrix properties.

This combined effect of whisker-related toughening and matrix-related toughening translating into a bulk fracture resistance has been rationalized for a sintered silicon nitride material (GTE AY6 grade).[76] Fracture toughness of the AY6 matrix depends on both grain size and shape as well as on the intergranular bond strength. In the SiC(w)/AY6-Si_3N_4 composites, considerable intergranular fracture and crack deflection with little evidence for bridging and pull-out were identified to account for the increase in fracture toughness observed. But it also became very obvious that matrix grain growth is affected due to incorporation of SiC-whiskers (see also Section 3.5).

The previous discussion indicates that even a qualitative evaluation of the interaction of nanometer-scale interfacial structures with fracture resistance in SiC(w)/Si_3N_4 composites defines a very challenging goal. The effect of the interfacial bond strength has been qualitatively addressed by comparing grain boundary configurations from both monolithic and composite Si_3N_4-based materials.[77]

The comparison of CVD-processed Si_3N_4 material with its hot-pressed or sintered cousins is a good example to emphasize the limits of this approach. CVD-Si_3N_4 is a polycrystalline material with high purity and density which exhibits no degradation in strength or fracture toughness beyond 1000°C. HREM investigations[78] revealed remarkably clean grain boundaries exhibiting direct bonding between matrix grains and no evidence for an amorphous interlayer or segregation of impurities. Obviously this type of grain boundary configuration will support integrity of the microstructure at high temperatures, but would the introduction of such 'strong' grain boundaries into a composite also result in improved fracture resistance? There is convincing evidence from several ceramic matrix-composite systems that the strong bonding will increase the amount of transgranular fracture, thus reducing the odds for interfacial boundaries to promote debonding or deflect a propagating crack.

This example emphasizes that a particular grain boundary configuration (direct bonding versus amorphous interlayers) defines a particular failure/toughening mechanism characterized by a bulk fracture resistance which is valid only for the particular matrix grain morphology and must not be extended *a priori* from a monolithic to a composite system. This fundamental aspect was recently demonstrated for two monolithic, liquid-phase sintered SiC and Si_3N_4 materials showing improved

toughnesses:[79] microcracking was revealed as the prevalent toughening mechanism for the SiC material with equiaxed grain morphology and perfectly clean grain boundaries. The Si_3N_4 material, characterized by exaggerated β-Si_3N_4 grain growth, however, was controlled by a crack-bridging mechanism supported by thin amorphous intergranular films which enable debonding.

The HREM/PEELS results discussed in Section 3.2 have provided new information about interfacial boundaries in SiC(w)/Si_3N_4. Recent HREM data from monolithic liquid-phase sintered Si_3N_4 materials utilizing different sintering aids[80] indicate that also the current understanding of grain and phase boundaries in the baseline material needs to be updated. It was revealed that the thickness of the amorphous interlayer for phase boundaries is always larger than observed for grain boundaries. This effect is independent of the additive composition, while the reverse is true for the film thickness of grain boundaries.

These results add another aspect of complexity to the correlation of microscopic (interfacial) properties to the fracture resistance of either monolithic or composite systems. Thus, the question which type of grain or phase boundary is addressed in a particular experiment or structure/property correlation will become more stringent as high-resolution TEM techniques provide more detailed information from these boundaries. The in-situ observation of crack propagation in a composite material is probably a suitable way out of this dilemma. Straining experiments of a SiC(w)/Al_2O_3 composite in a high-voltage TEM have been performed by Angelini *et al.*[81] which revealed the significance of debonding along the whisker periphery prior to failure. However, residual-stress-free thin TEM foils are not easily prepared. The different crack propagation in thin foils compared to bulk materials is considered an additional limitation of this approach.

In-situ experiments performed in a scanning electron microscope were pursued successfully by several research groups.[82,83] Although the SEM has its limits regarding access to structural information, in-situ testing of composites has outstanding capabilities with respect to real-time documentation of crack propagation, controlled fracture and even cyclic fatigue experiments.

Thus, in conclusion, it appears that the combined approach of utilizing HREM and analytical electron microscopy for a detailed characterization of interfaces in conjunction with in-situ experiments of composites in the SEM is an adequate method to reveal the fundamental aspects of micromechanical response from different types of grain and phase boundaries in ceramic matrix composites.

4 Conclusions

Interfacial boundaries in SiC(w)/Si_3N_4 composites have been investigated by means of HREM imaging and parallel detection electron energy loss spectroscopy (PEELS), focusing on the effect of oxygen segregation from different sources in the SiC/Si_3N_4 system. A discontinuous oxygen distribution was revealed from whisker/matrix interfaces, while a continuous oxygen-rich, nitrogen-depleted amorphous interlayer exists at β-Si_3N_4/β-Si_3N_4 matrix grain boundaries. Amorphous and crystalline regions were observed at SiC(w)/Si_3N_4 interfaces, which indicates that interfacial properties do not follow continuum mechanics models.

A significant difference in both structural and chemical interfacial width was derived from position-resolved electron loss spectroscopy. The chemical width exceeds the structural width by at least a factor of 10 because of a local dissolution of oxygen from the interfacial boundary into the β-Si_3N_4 matrix grain.

Although different SiC-whisker raw materials introduce local variations in interfacial roughness, periodicity and lateral widths of amorphous and crystalline regions along internal interfaces, the chemical interfacial width did not correlate with whisker-related oxygen concentrations, but rather represents an integral effect from different sources of oxygen during liquid-phase sintering of SiC(w)/Si_3N_4 compacts.

SiC reinforcement components like whiskers and platelets are introduced as non-stoichiometric, often polyphase components containing excess carbon and oxygen which affect the liquid-phase formation process in the Si_3N_4 system and thus matrix grain growth. Due to shifts in nominal composition oxygen may account for partial devitrification of the secondary phase.

It is demonstrated from different SiC-reinforced Si_3N_4 materials employing whiskers, platelets and fibers that interfacial boundaries are indeed dynamic features because of changes in the local microstructure due to thermodynamic constraints. The formation of reaction products such as graphite may strongly affect interfacial properties and mechanical response of ceramic composites. Due to surface energy changes the morphology of elongated SiC-whiskers may be metastable at high temperatures.

Whisker-related impurities are of minor significance to the fracture strength of SiC(w)/Si_3N_4 composites at room temperature. Morphology and size of SiC-whiskers are the critical parameters which affect the homogeneity of the microstructure and thus fracture strength.

The role of interfacial structures in the prevalent toughening mechanisms of Si_3N_4-based composites with discontinuous reinforcement components is discussed. Although it is recognized that all microscopic interfacial characteristics revealed by HREM and high-resolution analytical electron microscopy indeed contribute to the bulk fracture resistance of a SiC(w)/Si_3N_4 material, the whisker-related toughening effect is difficult to address in detail because of macroscopic matrix-related contributions to the mechanical response of the composites. A combined approach of high-resolution TEM techniques and in-situ testing of composite materials in a scanning electron microscope is suggested for further research on micromechanics of grain and phase boundaries in ceramic matrix composites.

Acknowledgement

HREM and PEELS data presented result from collaborative research on interfaces in structural ceramics between the Center For Solid State Science, Arizona State University, Tempe, AZ, USA and DLR, Materials Research Institute, Cologne, FRG. The constant support and dedication of R. W. Carpenter and K. D. Chowdhury during the last five years is gratefully acknowledged. Helpful discussions and critical comments to improve the structure of this paper were supplied by H. J. Kleebe, Max-Planck-Institut für Metallforschung, Stuttgart, FRG, which are greatly appreciated.

References

1. Rice, R. W., Mechanisms of toughening in ceramic matrix composites. *Ceram. Eng. Sci. Proc.*, **2** (1981) 661–701.
2. Marshall, D. B. & Evans, A. G., Failure mechanisms in ceramic-fiber/ceramic-matrix composites. *J. Am. Ceram. Soc.*, **68** (1985) 225–31.
3. Prewo, K. M., Fiber-reinforced ceramics: New opportunities for composite materials. *Am. Ceram. Soc. Bull.*, **68** (1989) 395–400.
4. Becher, P. F., Microstructural design of toughened ceramics. *J. Am. Ceram. Soc.*, **74** (1991) 255–69.
5. Claussen, N., Ceramic platelet composites. In *Proc. 11th Riso Int. Symp. on Metallurgy and Materials Science, Structural Ceramics, Processing, Microstructure and Properties*, Roskilde, DK, September 1990, pp. 1–12.
6. Kerans, R. J., Randall, S. H., Pagano, N. J. & Parthasarathy, T. A., The role of the fiber–matrix interface in ceramic composites. *Am. Ceram. Soc. Bull.*, **68** (1989) 429–42.
7. Rühle, M. & Evans, A. G., Structure and chemistry of metal/ceramic interfaces. *Mater. Sci. Eng.*, **A107** (1989) 187–97.
8. Fischmeister, H. F., Progress in understanding of ceramic microstructures and interfaces since 1976. In *Ceramic Microstructures '86, The Role of Interfaces*, ed. J. A. Pask & A. G. Evans. Plenum Press, New York, 1987, pp. 15–24.
9. Balluffi, R. W., Rühle, M. & Sutton, A. P., Special review: The structure of internal interfaces: Report of a discussion meeting. *Mater. Sci. Eng.*, **89** (1987) 1–16.
10. Clarke, D. R. & Wolf, D., Grain boundaries in ceramic and at ceramic–metal interfaces. *Mater. Sci. Eng.*, **83** (1986) 197–204.
11. Allard, L. F., Pendleton, P. & Brinen, J. S., Structure and chemistry of silicon carbide whisker surfaces. In *Proc. 44th Annual Meeting of the Electron Microscopy Society of America*, ed. G. Bailey. San Francisco Press, 1986, pp. 472.
12. Taylor, T. N., The surface composition of silicon carbide powders and whiskers: An XPS study. *J. Mater. Res.*, **4** (1989) 189–203.
13. Karasek, K. R., Bradley, S. A., Donner, J. T., Martin, M. R., Haynes, K. L. & Yeh, H. C., Composition and microstructure of silicon carbide whiskers. *J. Mat. Sci.*, **24** (1989) 1617–22.
14. Karasek, K. R., Bradley, S. A., Donner, J. T., Schienle, J. L. & Yeh, H. C., SiC whisker characterization: An update. *Am. Ceram. Soc. Bull.*, **70** (1991) 224–8.
15. Nutt, S. R., Microstructure and growth model for rice-hull derived SiC whiskers. *J. Am. Ceram. Soc.*, **71** (1988) 149–56.
16. Hölscher, A., Braue, W. & Ziegler, G., Mikrostrukturelle und oberflächenanalytische Charakterisierung keramischer Verstärkungskomponenten. *Mat.-wiss. u. Werkstofftech.*, **21** (1990) 120–8.
17. Iskoe, J. L. & Lange, F. F., Effect of selected impurities on the high temperature mechanical properties of hot-pressed silicon nitride. Westinghouse Research Labs, Report AD-783 506, 1974.
18. Meier, B., Hamminger, R. & Nold, E., Characterization of SiC platelets. *Mikrochim. Acta (Wien)*, **II** (1990) 195–205.
19. Saruhan, B., Braue, W. & Göring, J., Effect of SiC-platelets/-particles on microstructure and failure mechanism of silicon nitride composites. In *4th Intern. Symp. on Ceramic Materials and Components for Engines*, Göteborg, Sweden, 10–12 June 1991. Extended draft in preparation (1992).
20. Baril, D. & Mukesh, K. J., Evaluation of SiC platelets as a reinforcement for oxide matrix composites. *Ceram. Eng. Sci. Proc.*, **12** (1991) 1175–92.
21. Becher, P. F., Advances in the design of toughened ceramics. *J. Ceram. Soc. Japan*, **99** (1991) 993–1001.
22. Knippenberg, W. F., Growth phenomena in silicon carbide. *Philips Res. Repts*, **18** (1963) 161–274.
23. Kirchstein, G. & Koschel, D. (eds), *Gmelin Handbook of Inorganic Chemistry, 8th edn, Supplement, Volume B2 'Silicon'*. Springer-Verlag, 1986.
24. Boecker, W. D. G., Chwastiak, S., Frechette, F. & Lau, S. K., Single-phase alpha-SiC reinforcements for composites. In *Proceedings of the Silicon Carbide 1987 Symposium*, Columbus, OH, USA, 2–5 August 1987. The American Ceramic Society, 1989, pp. 407–20.
25. Shinozaki, S. & Kinsman, K. R., Aspects of 'one dimensional disorder' in silicon carbide. *Acta Metall.*, **26** (1978) 769–76.
26. Kleebe, H. J., Corbin, N., Wilkens, C. & Rühle, M., Transmission electron microscopy studies of silicon nitride/silicon carbide interfaces. *Mat. Res. Soc. Proc.*, **120** (1990) 79–84.
27. Koester, D. A., More, K. L. & Davis, R. F., Deformation and microstructural changes in SiC whisker-reinforced Si_3N_4 composites. *J. Mater. Res.*, **6** (1991) 2735–46.
28. Braue, W., Carpenter, R. W. & Smith, D. J., High-resolution interface analysis of SiC-whisker-reinforced Si_3N_4 and

Al_2O_3 ceramic matrix composite. *J. Mat. Sci.*, **25** (1990) 2949–57.
29. Campbell, G. H., Dalgleish, B. J, Rühle, M. & Evans, A. G., Whisker toughening: A comparison between Al_2O_3 and Si_3N_4 toughened with SiC. *J. Am. Ceram. Soc.*, **73** (1990) 521–30.
30. Carpenter, R. W., High resolution interface analysis. *Mater. Sci. Eng.*, **A107** (1989) 207–16.
31. Krivanek, O. L., Ahn, C. C. & Keeney, R. B., Parallel detection electron spectrometer using quadrupole lenses. *Ultramicroscopy*, **22** (1987) 103–16.
32. Weiss, J. K., Carpenter, R. W., Braue, W. & Higgs, A. A., Scanning probe parallel EELS analysis of interfaces in ceramics and ceramic composites. *Proc. 47th Annual Meeting of the Electron Microscopy Society of America*, ed. G. Bailey. San Francisco Press, 1989, pp. 226–7.
33. Carpenter, R. W., Chen, Y. Y., Kim, M. J. & Barry, J. C., Advances in the microscopy of processed semiconductors: Nanospectroscopy. *Micros. Semicond. Mater. Conf., Inst. Phys. Conf. Ser. No. 100, Section 7*, Oxford, 10–13 April 1989, pp. 543–50.
34. Chowdhury, K. D., Carpenter, R. W. & Braue, W., A Comparative high resolution study of interface chemistry in silicon nitride-based ceramic matrix composites reinforced with silicon carbide whiskers. *Ultramicroscopy*, **40** (1992) 229–39.
35. Chowdhury, K. D., Carpenter, R. W. & Braue, W., Analysis of oxygen distribution in interfaces in SiC-whisker-reinforced Si_3N_4-based composites. *Mat. Res. Soc. Symp. Proc.*, Fall Meeting 12/1991, in press.
36. Chowdhury, K. D., Carpenter, R. W. & Braue, W., in preparation (1992).
37. Schmidt, H. & Rühle, M., Structure of special grain boundaries in SiAlON ceramics. *J. Mater. Sci.*, **19** (1984) 615–28.
38. Clarke, D. R., Grain boundaries in polyphase ceramics. *J. de Physique Colloque*, **4** (1985) 51–9.
39. Clarke, D. R., On the equilibrium thickness of intergranular glass phases in ceramic materials. *J. Am. Ceram. Soc.*, **70** (1987) 15–22.
40. Ness, J. N. & Page, T. F., The structure and properties of interfaces in reaction-bonded silicon carbide. In *Tailoring Multiphase and Composite Ceramics, Proc. 21st University Conference on Ceramic Science*, University Park, PA/USA, 17–19 July 1985. Plenum Press, New York, 1986, pp. 347–56.
41. Niihara, K., Suganuma, K., Nakahira, A. & Izaki, K., Interfaces in Si_3N_4-SiC nanocomposites. *J. Mater. Sci. Lett.*, **9** (1990) 598–9.
42. Unal, O., Petrovic, J. J. & Mitchell, T. E., CVD-Si_3N_4 on single crystal SiC: Part I. Characterization and orientation relationship at the interface. *J. Mater. Res.*, **7** (1992) 136–47.
43. Alexander, K. B., Becher, P. F. & Waters, S. B., Characterization of silicon carbide platelet-reinforced alumina. In *Proc. XIIth International Congress for Electron Microscopy*, Seattle, Washington, USA, 12–18 August 1990. San Francisco Press, 1990, pp. 1032–3.
44. Homeny, J., Vaughn, W. L. & Ferber, M. K., Silicon carbide whisker/alumina matrix composites: Effect of whisker surface treatment on fracture toughness. *J. Am. Ceram. Soc.*, **73** (1990) 394–402.
45. Becher, P. F., Hsueh, C. H., Angelini, P. & Tiegs, T. N., Toughening behavior in whisker-reinforced ceramic matrix composites. *J. Am. Ceram. Soc.*, **71** (1988) 1050–61.
46. Wada, H., Wang, M. J. & Tien, T. T., Stability of phases in the Si–C–N–O system. *J. Am. Ceram. Soc.*, **71** (1988) 837–40.
47. Misra, A. K., Thermochemical analysis of chemical processes relevant to the stability and processing of SiC-reinforced Si_3N_4 composites. *J. Mater. Sci.*, **26** (1991) 6591–8.
48. Nickel, K. G., Hoffman, M. J., Greil, P. & Petzow, G., Thermodynamic calculations for the formation of SiC-whisker-reinforced Si_3N_4 ceramics. *Adv. Ceram. Mater.*, **3** (1988) 557–62.
49. Mah, T., Mendiratta, M. G., Katz, A. P. & Mazdiyasni, K. S., Recent developments in fiber-reinforced high temperature ceramic composites. *Am. Ceram. Soc. Bull.*, **66** (1987) 304–8.
50. Greil, P., Thermodynamic calculations of Si–C–O fiber stability in ceramic matrix composites. *J. Eur. Ceram. Soc.*, **6** (1990) 53–64.
51. Johnson, S. M., Brittain, R. D., Lamoreaux, R. H. & Rowcliffe, D. J., Degradation mechanisms of silicon carbide fibers. *J. Am. Ceram. Soc.*, **71** (1988) C132–C135.
52. Schoenlein, L. H., Jones, R. H., Henager, C. H., Schilling, C. H. & Gac, F., Interfacial chemistry—structure and fracture of ceramic composites. *Mater. Res. Soc. Symp.*, **120** (1988) 313–21.
53. Chaim, R. & Heuer, A. H., Carbon interfacial layers formed by oxidation of SiC in SiC/Ba-stuffed cordierite glass–ceramic reaction couples. *J. Am. Ceram. Soc.*, **74** (1991) 1663–7.
54. Cooper, R. F. & Chyung, K., Structure and chemistry of fibre–matrix interfaces in silicon carbide fibre-reinforced glass–ceramic composites: An electron microscopy study. *J. Mater. Sci.*, **22** (1987) 3148–60.
55. Luthra, K. L., Chemical interactions in high-temperature ceramic composites. *J. Am. Ceram. Soc.*, **71** (1988) 1114–20.
56. Shaw, M. C. & Faber, K. T., Temperature-dependent toughening in whisker-reinforced ceramics. In *Ceramics Microstructures '86, The Role of Interfaces*, ed. J. A. Pask & A. G. Evans. Plenum Press, New York, 1987, pp. 929–38.
57. Hong, J. D., Hon, M. H. & Davis, R. F., Self diffusion in alpha- and beta-silicon carbide. *Ceramurg. Int.*, **5** (1979) 155–60.
58. Ning, X. J. & Pirouz, P., The microstructure of SCS-6 SiC fiber. *J. Mater. Res.*, **6** (1991) 2234–48.
59. Zhou, Y. C. & Xia, F., Effect of processing temperature on the morphology of silicon carbide whiskers. *J. Am. Ceram. Soc.*, **74** (1991) 447–9.
60. Hollar, W. E. & Kim, J. J., Review of VLS SiC whisker growth technology. *Ceram. Eng. Sci. Proc.*, **12** (1991) 979–91.
61. Porter, R. L., Plasma-induced morphological changes in alpha-silicon carbide. *J. Am. Ceram. Soc.*, **70** (1987) C26–C28.
62. Watari, K., Kawamoto, M. & Ishizaki, K., Carbon behavior in sintered silicon nitride grain boundaries. *Mater. Sci. Eng.*, **A109** (1989) 89–95.
63. Tanaka, H., Greil, P. & Petzow, G., Sintering and strength of silicon nitride/silicon carbide composites. *Int. J. High Tech. Ceram.*, **1** (1985) 107–18.
64. Wötting, G., Kanka, B. & Ziegler, G., Microstructural development, microstructural characterization and relation to mechanical properties of dense silicon nitride. In *Non-Oxide Technical and Engineering Ceramics*, ed. St. Hampshire. Elsevier Applied Science, London/New York, 1986, pp. 83–96.
65. Handwerker, C. A., Morris, P. A. & Coble, R. L., Effects of chemical inhomogeneities on grain growth and microstructure in Al_2O_3. *J. Am. Ceram. Soc.*, **72** (1989) 130–6.
66. Kaysser, W. A., Sprissler, M., Handwerker, C. A. & Blendell, J. E., The effect of a liquid phase on the morphology of grain growth in alumina. *J. Am. Ceram. Soc.*, **70** (1987) 339–43.
67. Braue, W., Hölscher, A., Saruhan, B. & Ziegler, G., Effect of SiC-whisker characteristics on interface and mechanical properties of silicon nitride matrix composites. *Proc. 1st Eur. Ceramic Soc. Conf./Sci. Ceram. 15*, Maastricht, The Netherlands, 18–23 June 1989. Elsevier Applied Science, 1989, pp. 3.263–3.267.
68. Evans, A. G., Rühle, M., Dalgleish, B. J. & Thouless, M. D.,

On prevalent whisker toughening in ceramics. *Mater. Res. Soc. Symp.*, **78** (1987) 259–71.
69. Rühle, M. & Evans, A. G., High toughness ceramics and ceramic composites. *Prog. Mater. Sci.*, **33** (1989) 85–167.
70. Gac, F. D., Is there anything of practical value hidden amongst the composite-toughening theories?!—A Jim Mueller perspective. *Ceram. Eng. Sci. Proc.*, **11** (1990) 551–70.
71. Rice, R. W., Toughening in ceramic particulate and whisker composites. *Ceram. Eng. Sci. Proc.*, **11** (1990) 667–94.
72. Evans, A. G., Perspective on the development of high-toughness ceramics. *J. Am. Ceram. Soc.*, **73** (1990) 187–206.
73. Chaim, R. & Heuer, A. H., The interface between (Nicalon) SiC fibers and a glass–ceramic matrix. *Adv. Ceram. Mater.*, **2** (1987) 154–8.
74. Bischoff, E., Rühle, M., Sbaizero, O. & Evans, A. G., Microstructural studies of the interfacial zone of a SiC-fiber-reinforced lithium aluminium silicate glass–ceramic. *J. Am. Ceram. Soc.*, **72** (1989) 741–5.
75. Thouless, M. D., Sbaizero, O., Sigl, L. S. & Evans, A. G., Effect of interface mechanical properties on pullout in SiC-fiber-reinforced lithium–aluminium silicate glass–ceramic. *J. Am. Ceram. Soc.*, **72** (1989) 525–32.
76. Buljan, S. T., Baldoni, J. G., Huckabee, M. L. & Zilberstein, G., Microstructure and fracture toughness of silicon nitride composites. In *Whisker- and Fiber-Toughened Ceramics, Proceedings of an International Conference*, Oak Ridge, TN, USA, 7–9 June 1988, pp. 113–23.
77. Niihara, K., Mechanical properties of chemically vapor deposited nonoxide ceramics. *Am. Ceram. Soc. Bull.*, **63** (1984) 1160–3.
78. Hiraga, K., Application of high-resolution electron microscopy to the study of structure defects and grain boundaries in Si_3N_4 and SiC. *Sci. Rep. Res. Inst. Tohoku Univ. Ser. A*, **32** (1984) 1–20.
79. Kleebe, H. J., Si_3N_4 and SiC materials with improved fracture resistance. *J. Eur. Ceram. Soc.*, this issue.
80. Kleebe, H. J. & Rühle, M., Analytical electron microscopy and high-resolution electron microscopy studies of grain boundary films in silicon nitride-based ceramics. *Mater. Res. Soc. Symp. Proc.*, 12/1991, in press.
81. Angelini, P., Mader, W. & Becher, P. F., Strain and fracture in whisker reinforced ceramics. *Mater. Res. Soc. Symp. Proc.*, **78** (1987) 241–57.
82. Frei, H. & Grathwohl, G., New test methods for engineering ceramics—In-situ microscopy investigation. *Ceramic Forum International/Ber. DKG*, **68** (1991) 27–35.
83. Rödel, J., Fuller, E. R. & Lawn, B. R., In-situ observations of toughening processes in alumina reinforced with silicon carbide whiskers. *J. Am. Ceram. Soc.*, **74** (1991) 3154–7.